

1 Supplementary material

The figures included in this section are intended to be shown at conferences.

Figs. 1 and 2 show the distributions of the $\mathcal{M}_{3\text{body}}$ and \mathcal{M}_{PID} (for $\tau^- \rightarrow \mu^- \mu^+ \mu^-$ only) likelihoods for simulated signal events and data sidebands, as binned in the analysis and normalised to 1. The response of the simulated signal events after calibration according to data is also shown.

Fig. 3 shows the distribution of simulated $\tau^- \rightarrow \mu^- \mu^+ \mu^-$ signal events in bins of $\mathcal{M}_{3\text{body}}$ and \mathcal{M}_{PID} after calibration. This is useful to illustrate the binning scheme shown in mass plots.

Fig. 4 shows the large contribution of $D_s^- \rightarrow \eta(\mu^+ \mu^- \gamma) \mu^- \bar{\nu}_\mu$ events to the total background in the merged four highest likelihood bins for the $\tau^- \rightarrow \mu^- \mu^+ \mu^-$ analysis, prior to the cut at $450 \text{ MeV}/c^2$ on the $\mu^+ \mu^-$ mass. This motivates the cut on the dimuon mass.

Fig. 5 shows the peaking background in the data sidebands from the misidentification of $D^+ \rightarrow K^- \pi^+ \pi^+$ events in the lowest bin of \mathcal{M}_{PID} . This motivates the exclusion of the lowest likelihood bins from the limit calculation.

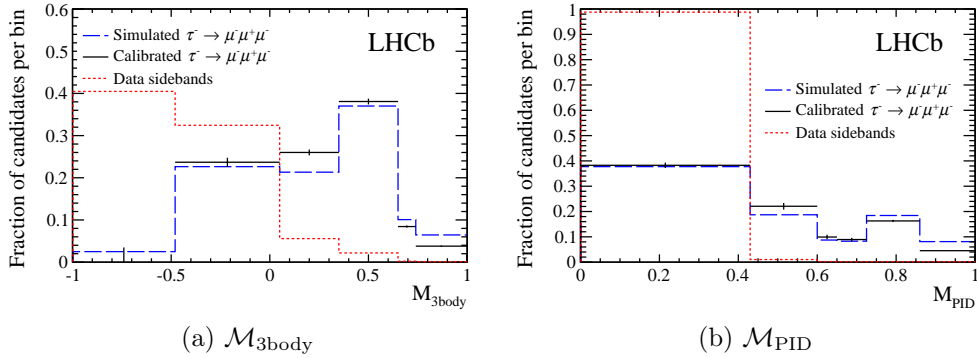


Figure 1: Distribution of (a) $\mathcal{M}_{3\text{body}}$ and (b) \mathcal{M}_{PID} for simulated signal events and data sidebands for $\tau^- \rightarrow \mu^- \mu^+ \mu^-$.

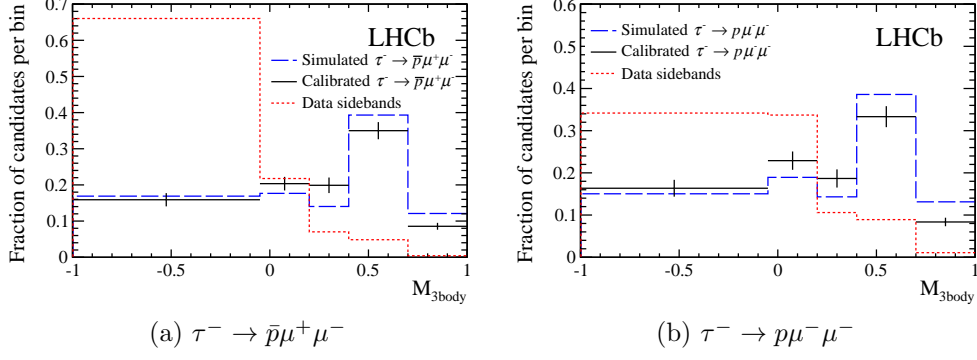


Figure 2: Distribution of $\mathcal{M}_{3\text{body}}$ for simulated signal events and data sidebands for (a) $\tau^- \rightarrow \bar{p}\mu^+\mu^-$ and (b) $\tau^- \rightarrow p\mu^-\mu^-$.

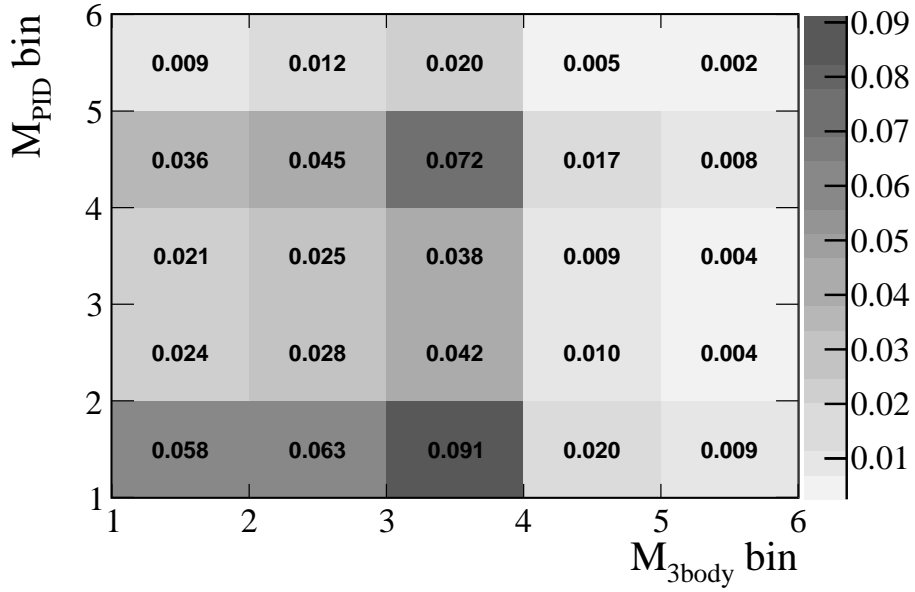


Figure 3: Distribution of simulated signal events in the $\mathcal{M}_{3\text{body}}$ and \mathcal{M}_{PID} bins used in the analysis for $\tau^- \rightarrow \mu^-\mu^+\mu^-$.

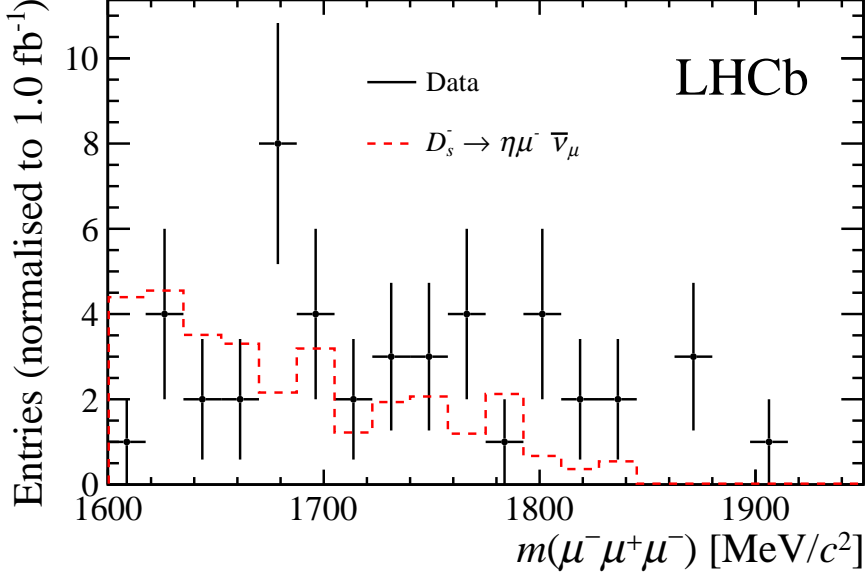


Figure 4: Contribution of $D_s^- \rightarrow \eta(\mu^+\mu^-\gamma)\mu^-\bar{\nu}_\mu$ (dashed line) decays to the total background (points with error bars) in the merged highest likelihood bins ($\mathcal{M}_{3\text{body}} > 0.65$ and $\mathcal{M}_{\text{PID}} > 0.725$) for $\tau^- \rightarrow \mu^-\mu^+\mu^-$ as determined from simulation, where the simulated events are normalised to 1.0 fb^{-1} .

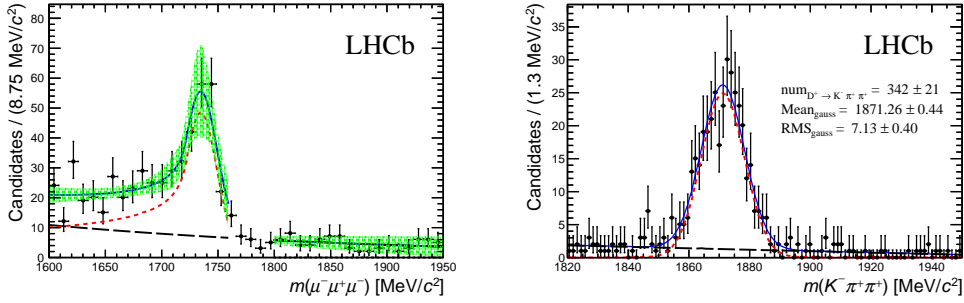


Figure 5: Left: Fit to the data sidebands for the bin $0.74 < \mathcal{M}_{3\text{body}} < 1.0$ and $0.0 < \mathcal{M}_{\text{PID}} < 0.43$ for $\tau^- \rightarrow \mu^-\mu^+\mu^-$. The fine dashed line indicates the Crystal Ball function describing the $D^+ \rightarrow K^-\pi^+\pi^+$ background, the thick dashed line the exponential background and the solid line the total fit function. Right: Fit to the data sidebands for the bin $0.74 < \mathcal{M}_{3\text{body}} < 1.0$ and $0.0 < \mathcal{M}_{\text{PID}} < 0.43$ under the $K^-\pi^+\pi^+$ mass hypothesis. The fine and thick dashed lines indicate the Gaussian and Chebychev polynomial components, respectively.